Available online at www.sciencedirect.com
ScienceDirect
Journal of Sound and Vibration 307 (2007) 778–801
JOURNAL OF SOUND AND VIBRATION
www.elsevier.com/locate/jsvi

Dynamics of an unconstrained oscillatory flicking brush for road sweeping

L.V. Vanegas Useche[1], M.M. Abdel Wahab*, G.A. Parker

Faculty of Engineering and Physical Sciences (J5), University of Surrey, Guildford GU2 7XH, UK

Received 12 September 2006; received in revised form 6 July 2007; accepted 9 July 2007
Available online 22 August 2007

Abstract

This article studies the dynamics of a freely rotating flicking brush by means of a mathematical model. The bristles are treated as cantilever prismatic beams subjected to small deflections. A solution of the equation of motion for their forced transverse vibration is obtained through the normal-mode method. A novel oscillatory motion is superimposed onto the rotary motion of the brush. Two functions of oscillation are investigated: a sinusoidal angular velocity and a novel function, named after the authors 'VAP' (Vanegas Useche, Abdel Wahab, Parker), developed to provide small shaft accelerations. The VAP function may be a square wave, a triangle wave, or a smooth wave between them, depending on the value of a smoothness parameter, b. The results indicate that the maximum bending moment, stress, and deflection are independent of the mean angular velocity, are proportional to its alternating component, and increase linearly with the mount radius and the sine of the mount angle. In addition, the behaviour of the brush is strongly affected by the frequency of oscillation, the type of function, the value of b, and bristle wear, amongst other parameters. For the sinusoidal and VAP function, resonance occurs at the bristle natural frequencies. Moreover, the VAP function tends to produce a condition similar to resonance also at odd fractions of the natural frequencies. This phenomenon may be accentuated or reduced, by adjusting the value of b, and be expedited or impeded, by the selection of the frequency. The results of this work may also be applied to the case of a small-deflection cantilever beam, when the transverse external force is a sinusoidal, square, or triangle wave or when it is given by the new VAP function. Finally, the VAP wave may enable to excite a condition similar to resonance not only at the natural frequencies of the beam, but also at odd fractions of them. Small frequencies may be required to achieve a resonant behaviour of a high-frequency mode; this behaviour can be controlled by means of the smoothness parameter.

1. Introduction

Street sweepers usually operate with a small gutter brush, which sweeps the debris that lies in the gutter towards the path of a wide broom or a suction unit. As shown in Fig. 1, the bristles of gutter brushes are grouped into one or more rows of clusters and are attached to the mounting board with a cup-like form. The bristles are usually of steel, cold drawn or hardened and tempered, or polypropylene. Commonly, there are

*Corresponding author. Tel.: +44 1483 689615; fax: +44 1483 306039.
E-mail address: m.wahab@surrey.ac.uk (M.M. Abdel Wahab).
[1]On leave from Facultad de Ingeniería Mecánica, Universidad Tecnológica de Pereira, La Julita, Pereira, Colombia.

0022-460X/$ - see front matter © 2007 Elsevier Ltd. All rights reserved.
doi:10.1016/j.jsv.2007.07.010

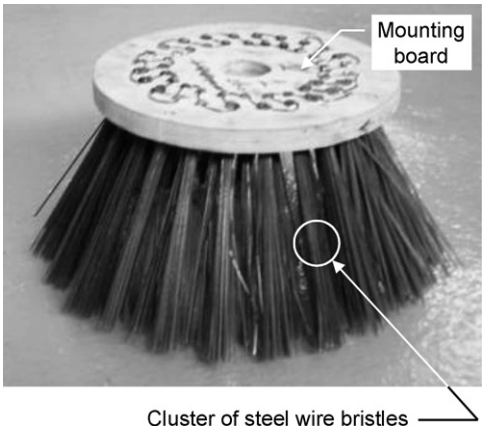

Fig. 1. Flicking brush of a street sweeper.

two types of brushes: the cutting brush, whose bristles deflect mainly in the brush radial direction producing a stiff collision with the debris, and the flicking brush, whose bristles deform predominantly in the tangential direction. It is generally accepted that gutter brushes sweep about 80% of the debris, which is found in the gutter [1]; therefore, their performance is important. Despite this fact, the amount of research on gutter brushes is very limited.

Research into brushing technology suggests that when brush oscillations are superimposed onto brush rotation, brushing efficiency and the coefficient of friction between the bristle tips and the contacting surface are affected. For instance, a comprehensive review of the efficiency of powered toothbrushes indicates that oscillating–rotating toothbrushes are the only type of brush that consistently shows better performance than manual brushes. It has been concluded that they lead to 17% less gingivitis and remove around 7% more plaque than the manual ones [2]. Similarly, it has been found that back-and-forth oscillations of a polyvinyl alcohol (PVA) brush for post-chemical–mechanical polishing (CMP) scrubbing process, along with a rotation of the wafer, have a dramatic impact on the coefficient of friction and, thus, on brushing efficiency [3]. It is shown that the coefficient of friction remains fairly constant for low rotational speeds, but it is greatly increased for high speeds.

In the light of the above, it is of interest to investigate the effect of brush oscillations on the dynamics and performance of a gutter brush. This is a novel concept that is being investigated at the University of Surrey. In order to gain an insight into the behaviour of oscillatory gutter brushes, it is convenient to achieve first an understanding of the influence of a variable angular speed on the dynamics of the brush during free rotation, as the effects of brush oscillations of a constrained brush tend to be damped by the road surface and the problem requires more complex models. The primary aims of this investigation are (a) to develop an analytical model for the dynamics of the bristles of an unconstrained flicking brush subjected to an oscillating rotational speed; (b) to identify the parameters that affect the most or otherwise the sweeping process and how these parameters, as well as their interaction, affect brush behaviour; (c) to gain an understanding of the effects of brush oscillations on bristle deflections, stresses, and vibration patterns, when the brush operates in free flight. The bristle is modelled as a continuous system, and its forced response is determined through the normal-mode method. The variable rotational speed of the brush is either a sinusoidal function or a new function, named VAP (named after the authors, Vanegas Useche, Abdel Wahab, Parker). The VAP function has been devised so as to provide small accelerations of the brush shaft. However, its shape can be varied from a square wave to a triangle wave, depending on the value of a smoothness parameter, b. Therefore, the model also provides an understanding of the behaviour of a brush under different functions of oscillation. Particular emphasis is placed on studying the response of the bristle to the VAP excitation for the whole range of the smoothness parameter. The results presented in this work can also be extended to the case of the transverse vibrations of a small-deflection 2-D (two-dimensional) cantilever beam.

2. Related work

In spite of the important role that gutter brushes play in the sweeping practice, published research on gutter brushes of street sweepers is very limited [1,4–9]. These works study the dynamics and performance of cutting and/or flicking brushes, as well as the automation of the brushing process. In Peel et al. [1], Peel [4], and Peel and Parker [5], parameters such as forces and torques in a horizontal or tilted brush acting against flat surfaces (e.g., oil-lubricated steel and motorway grade concrete) are analysed by means of experimental tests and a large-deflection static discrete model [10]. In the model, it is assumed that the bristles in a given cluster are subjected to the same deflections and loads, that the bristles deform only in the "weaker" plane for bending deflections (2-D analysis), and that there is no interaction among bristles. The model takes into consideration the centrifugal forces but neglects any other inertia forces, gravity, and aerodynamic forces. Similarly, Wang [7] studies the characteristics of gutter brushes by means of finite element models. These models constitute an improvement on previous investigations [1,4,5], because they calculate 3-D bristle deformations. In addition, Vanegas et al. [8] present preliminary results of the behaviour of oscillatory, unconstrained cutting brushes. Comparisons between the results of the present work and those in Ref. [8] are provided throughout the article. Lastly, Vanegas et al. [6] present preliminary results of the behaviour of oscillatory, unconstrained flicking brushes for the case of a bristle mount angle equal to zero. The results of these works [1,4–8] on gutter brushes demonstrate the complexities involved in their study, as their characteristics depend on the interaction of many variables such as penetration, rotational speed, angle of attack, coefficient of friction, bristle length, and vehicle velocity and phenomena such as stick–slip friction cycles. The reader is referred to Ref. [9], which reviews gutter brush dynamics.

On the other hand, a study of freely rotating straight cup brushes for surface finishing operations has been carried out by Stango and Shia [10]. The deformation characteristics of the bristles of circular cross-section are analysed by means of a large-deflection discrete static model. The beam is modelled as a number of straight, rigid elements interconnected through torsional springs. It is assumed that there is no interaction among bristles and that they are uniformly distributed, of equal length, and initially straight. It is also assumed that the bristles withstand no deformation along the bristle length and that there is no eccentricity of the brush. Additionally, gravity and aerodynamic forces are neglected. The results indicate that the maximum stress, which occurs at the clamped end, the filament tip angle and displacement, and the operating brush diameter increase with the rotational speed of the brush and the bristle mount radius. Through an example, it is shown that the centrifugal forces on their own, i.e., without brush penetration, commonly produce high stress levels. This is due to the high rotational speeds of cup brushes (e.g., 3600 rev/min). The results also indicate that due to the different mount radii of the bristles, the centrifugal forces cause variable tip spacing along the radial direction of the brush and different distances from the bristle tips to a hypothetical surface. This will tend to affect the surface finish of the workpart and the percentage of bristles in contact with it, when the brush is subjected to penetration. Furthermore, large penetrations are required for high rotational speeds in order that all the bristles make contact with the surface and that the brushing forces are sufficiently high. Therefore, the stresses in constrained cup brush tend to be very high.

Finally, study of the dynamics of beams attached to moving supports has been pursued for several decades. Many researches have developed dynamic models for beams attached to a rotating base (e.g., Refs. [11–13]) or undergoing large overall motions (e.g., Refs. [14,15]). The beam models are linear or nonlinear and may consider, for example, axial extension, torsion, shear displacements, warping, and centrifugal stiffening (e.g., Ref. [14]). Classic linear modelling is simple and easy to apply in finite element methods, but the accuracy is compromised when the beam undergoes large overall motions [15]. Conversely, nonlinear models are more complex and computationally less efficient, but they tend to be more accurate. However, Yoo et al. [15] and Chung and Yoo [16] develop accurate linear models based on a stretch deformation variable, which captures motion-induced stiffness variations, and the linearization of the problem reduces computational effort. These comprehensive models have applicability in cases such as turbine blades, aircraft rotary wings, and helicopter rotor blades, where high rotational speeds and/or large overall motions are involved.

3. Kinematic analysis and assumptions

A flicking brush is a type of gutter brush whose bristles are of rectangular cross-section and are orientated so that they mainly deflect in the tangential direction, as illustrated in Fig. 2. Because of this, the contact between the bristles and the debris tends to be smooth (compared with the stiff collisions in a cutting brush). However, the bristle is released from the road surface at relatively high speed, providing a flicking action. In this work, the novel concept of an oscillatory flicking brush is studied. Therefore, the brush rotation is characterised by a variable angular velocity, ω, and angular acceleration, α. The bristles are fixed to the mounting board at an angle ϕ with respect to the axis of rotation (z_b). This angle is called the bristle mount angle. The frame $x_G y_G z_G$ is assumed to be a fixed Cartesian coordinate system, and the systems $x_b y_b z_b$ and xyz are fixed to the brush.

The top end of the bristle (A) is clamped to the mounting board and, thus, performs a circular motion with a variable angular velocity. Hence, point A has both a normal component and a tangential component of acceleration, which are variable. The accelerations along the bristle, the aerodynamic forces, and gravity produce complex patterns of bristle vibrations. The bristle withstands transverse vibrations in the xy plane, which constitutes the weaker plane for bending deflections, transverse vibrations in the xz plane (stronger plane), and torsional vibrations, whose interaction is difficult to model theoretically.

In the light of this difficulty, the model derived in this article assumes that the bristle does not twist, is subjected to small deflections, and vibrates only in the weaker plane. It is also assumed that the bristles are rigidly clamped into the mounting board, that there is no interaction among bristles, and that they withstand the same loads and deflections. In addition, shear deformations, rotary inertia, gravity, aerodynamic forces, and internal damping are neglected. These assumptions are considered appropriate in this case, due to the slenderness of the bristle, the value of the aspect ratio of the cross-section, and the low rotational speeds of gutter brushes. In addition, experimental results on gutter brushes indicate that most of these assumptions provide valid results [4].

The kinematics of the bristle is studied through relative-motion analysis using rotating axes. The brush system of axes $x_b y_b z_b$ is a rotating system characterised by ω and α, and it has a fixed origin, O, which

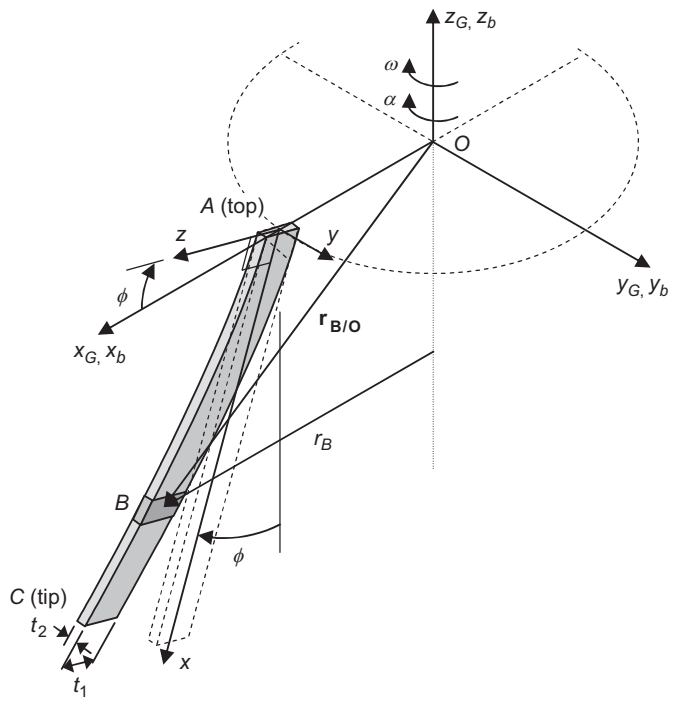

Fig. 2. Representation of a bristle of an oscillatory flicking brush.

coincides with the origin of the global coordinate system. Thus, the acceleration vector of any element B (Fig. 2) can be expressed with reference to the rotating system:

$$\mathbf{a}_B = \mathbf{a}_O + \boldsymbol{\alpha} \times \mathbf{r}_{B/O} + \boldsymbol{\omega} \times (\boldsymbol{\omega} \times \mathbf{r}_{B/O}) + 2(\boldsymbol{\omega} \times \mathbf{v}_{B_{\text{rel}}}) + \mathbf{a}_{B_{\text{rel}}}, \tag{1}$$

where $\mathbf{r}_{B/O}$ is the position vector of B with respect to O and $\mathbf{v}_{B_{\text{rel}}}$ and $\mathbf{a}_{B_{\text{rel}}}$ are the velocity and acceleration of B relative to the rotating coordinate system, respectively. However, the acceleration of point O, $\mathbf{a}_O$, is zero. The angular velocity and angular acceleration vectors of the coordinate system $x_b y_b z_b$ are given by

$$\boldsymbol{\omega} = \omega(-\mathbf{k}_G) \quad \text{and} \quad \boldsymbol{\alpha} = \alpha(-\mathbf{k}_G), \quad \text{where} \quad \alpha = \frac{\mathrm{d}\omega}{\mathrm{d}t}, \tag{2}$$

$\mathbf{k}_G$ is a unit vector acting in the z_G direction, and t is time. Due to the assumptions made, point B virtually performs a rectilinear motion in the y direction. Therefore, it has that

$$\mathbf{v}_{B_{\text{rel}}} = v_{B_{\text{rel}}}\mathbf{j} = \frac{\mathrm{d}y}{\mathrm{d}t}\mathbf{j} \quad \text{and} \quad \mathbf{a}_{B_{\text{rel}}} = a_{B_{\text{rel}}}\mathbf{j} = \frac{\mathrm{d}^2 y}{\mathrm{d}t^2}\mathbf{j}, \tag{3}$$

where y is the deflection of point B and $\mathbf{j}$ is a unit vector in the y direction. Thus, taking into account that for small deflections the y_G component of the position vector of B can be neglected (Fig. 2), Eq. (1) can be expressed as

$$\mathbf{a}_B = \alpha r_B(-\mathbf{j}_G) + \omega^2 r_B(-\mathbf{i}_G) + 2\omega v_{B_{\text{rel}}}\mathbf{i}_G + a_{B_{\text{rel}}}\mathbf{j}$$

or by noting in Fig. 2 that $\mathbf{j}_G = \mathbf{j}$ and $\mathbf{i}_G = \sin\phi\mathbf{i} + \cos\phi\mathbf{k}$,

$$\mathbf{a}_B = -\alpha r_B\mathbf{j} - \omega^2 r_B(\sin\phi\mathbf{i} + \cos\phi\mathbf{k}) + 2\omega v_{B_{\text{rel}}}(\sin\phi\mathbf{i} + \cos\phi\mathbf{k}) + a_{B_{\text{rel}}}\mathbf{j}, \tag{4}$$

where r_B (Figs. 2 and 3) is the perpendicular distance from B to the z_G axis and $\mathbf{i}_G$, $\mathbf{j}_G$, $\mathbf{i}$, and $\mathbf{k}$ are unit vectors in the x_G, y_G, x, and z directions, respectively. From Fig. 3, r_B is given by

$$r_B = r_A + x\sin\phi, \tag{5}$$

where r_A is the bristle mount radius.

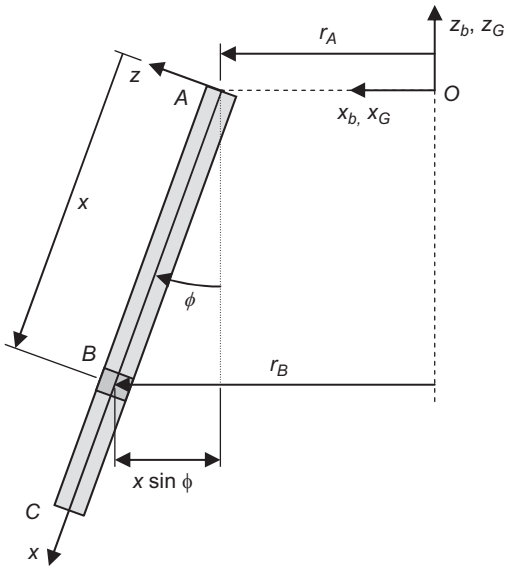

Fig. 3. xz view of the bristle.

4. Analytical model

The bristle of the oscillatory flicking brush is considered to be in dynamic equilibrium. Then, the acceleration of every element of the bristle can be dealt with by subjecting the element to an equivalent inertial force. Nevertheless, only the y component of acceleration is required, as it has been assumed that the bristle elements move only in the y direction. From Eqs. (3) and (4), the y component of acceleration is given by

$$a_{B_y} = -\left(\alpha r_B - \frac{\mathrm{d}^2 y}{\mathrm{d}t^2}\right). \tag{6}$$

This acceleration is converted into an inertia force per unit length, q, acting along the bristle and whose direction is opposite to that of the acceleration, as shown in Fig. 4. Through the use of Eqs. (5) and (6), the inertia force can be expressed as

$$q = \frac{\mathrm{d}m}{\mathrm{d}x}\left(-a_{B_y}\right) = \rho A\left(a_t - \frac{\mathrm{d}^2 y}{\mathrm{d}t^2}\right), \quad \text{where} \quad a_t = \alpha(r_A + x\sin\phi) \tag{7}$$

and m, ρ, and A are the mass, the density, and the cross-sectional area of the bristle, respectively. Fig. 4 shows the static model of the vibration of the bristle, where A is a built-in, fixed point in the xyz system.

To investigate the transverse vibration of this continuous system, Fig. 5 presents the free-body diagram of an element B of length $\mathrm{d}x$. From the formulation of the dynamic equilibrium equations of the element in Fig. 5, first-order bending theory, and Eq. (7), it has that

$$-\frac{\partial^2 M_z}{\partial x^2} = \rho A\frac{\partial^2 y}{\partial t^2} - \rho A a_t, \tag{8}$$

where M_z is the bending moment of the bristle element at a distance x from the top end at time t. From first-order bending theory, it has that

$$M_z = EI_{zz}\frac{\mathrm{d}^2 y}{\mathrm{d}x^2}, \tag{9}$$

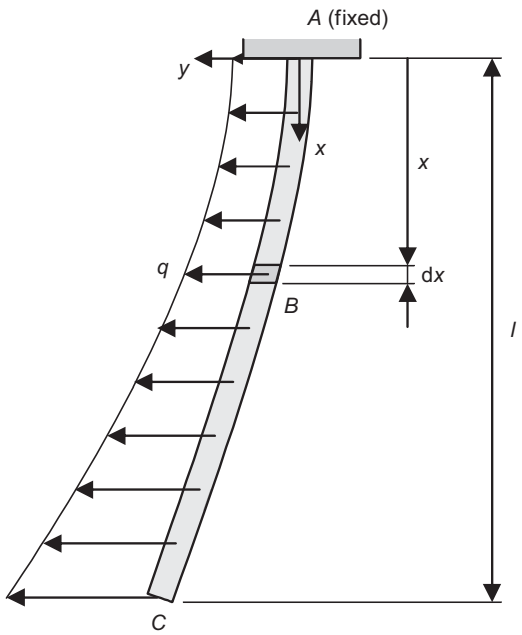

Fig. 4. Static model of bristle vibration.

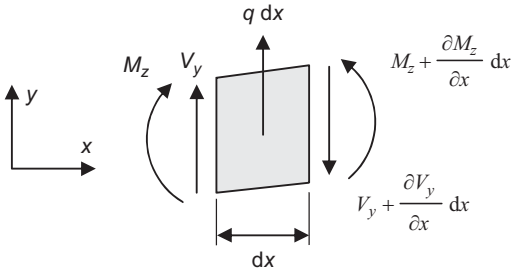

Fig. 5. Free-body diagram of an infinitesimal element of the bristle.

where E is the Young's modulus and I_{zz} is the second moment of area of the bristle. Hence, Eq. (8) yields

$$-\frac{\partial^4 y(x,t)}{\partial x^4} = \frac{1}{k_a^2}\frac{\partial^2 y(x,t)}{\partial t^2} - \frac{1}{k_a^2}a_t(x,t), \quad \text{where} \quad k_a^2 = \frac{EI_{zz}}{\rho A}. \tag{10}$$

Eq. (10) is the well-known linear, partial, fourth-order differential equation of motion for the forced transverse vibration of a beam. By using the normal-mode method and the Duhamel integral [17], and by applying the boundary conditions (i.e., zero deflection and slope at $x = 0$ and zero bending moment and shearing force at $x = l$), a solution of this equation is

$$y = \sum_{i=1}^{\infty}\left\{2h_i(t)\left(\frac{C_{4i}}{k_i} - \frac{C_{2i}}{k_i^2}\frac{\sin\phi}{r_A}\right)\frac{C_{2i}(\cos k_i x - \cosh k_i x) + C_{4i}(\sin k_i x - \sinh k_i x)}{\omega_i}\right\}, \tag{11}$$

where

$$k_i^2 = \frac{\omega_i}{k_a} = \omega_i\sqrt{\frac{\rho A}{EI_{zz}}}, \tag{12}$$

$$\cos k_i l \cosh k_i l = -1, \quad C_{4i} = -C_{2i}\left(\frac{\cos k_i l + \cosh k_i l}{\sin k_i l + \sinh k_i l}\right), \quad C_{2i} = l^{-1/2}, \tag{13}$$

$$h_i(t) = \int_0^t r_A \alpha(t')\sin[\omega_i(t - t')]\,dt', \tag{14}$$

where l is the bristle length, ω_i is the frequency of the ith natural mode ($i = 1{-}\infty$), and t' is a dummy time variable.

The bending moment along the bristle can be determined by differentiating twice Eq. (11) and substituting the resultant expression into Eq. (9). This yields

$$M_z = -2EI_{zz}\sum_{i=1}^{\infty}\left\{h_i(t)\left(C_{4i}k_i - C_{2i}\frac{\sin\phi}{r_A}\right)\frac{C_{2i}(\cos k_i x + \cosh k_i x) + C_{4i}(\sin k_i x + \sinh k_i x)}{\omega_i}\right\}. \tag{15}$$

The natural frequency, f_i, and natural period, τ_i, can be obtained from Eq. (12)

$$f_i = \frac{1}{\tau_i} = \frac{\omega_i}{2\pi} = \frac{k_i^2}{2\pi}\sqrt{\frac{EI_{zz}}{\rho A}} = \frac{(k_i l)^2}{2\pi}\sqrt{\frac{EI_{zz}}{\rho A l^4}}. \tag{16}$$

Lastly, it is necessary to solve the integral in Eq. (14), which depends on the angular acceleration of the brush, in order to obtain a complete solution. As mentioned in Section 1, two angular acceleration functions, $\alpha(t)$, are considered: a sinusoidal function and the VAP function, which has been developed by the authors to obtain small shaft accelerations. The sinusoidal angular velocity and acceleration can be expressed as

$$\omega(t) = \omega_m + \omega_a \sin 2\pi f t \quad \text{and} \quad \alpha(t) = 2\pi f \omega_a \cos 2\pi f t, \tag{17}$$

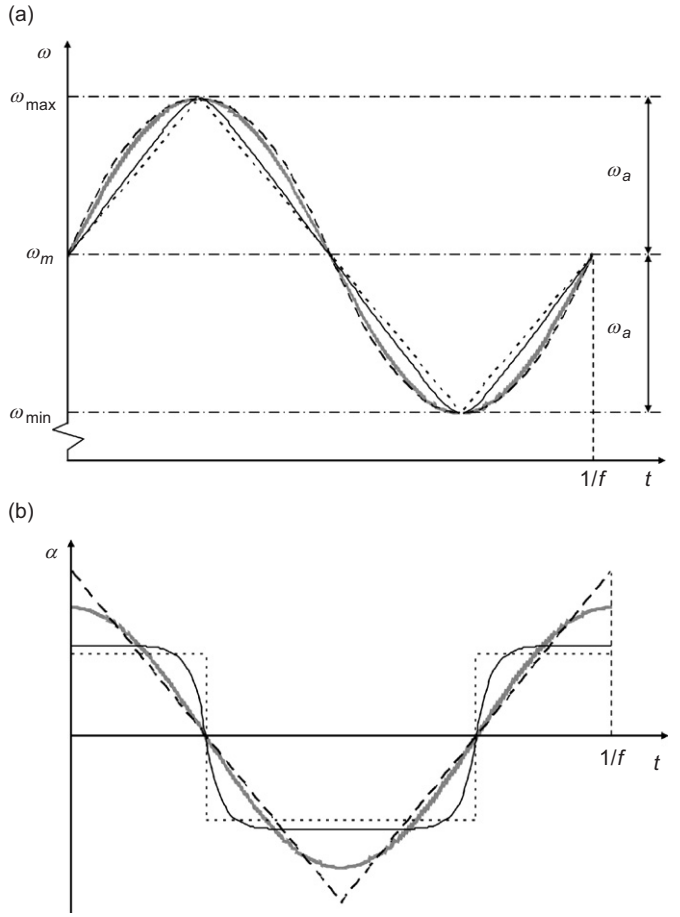

Fig. 6. Angular velocity and acceleration curves for the sinusoidal and VAP function: (a) angular velocity against time, (b) angular acceleration against time. ıılıılıılıı sinusoidal, - - - - VAP with $b \approx 0$, — VAP with $b = 0.1$, – – · VAP with $b \approx 1$.

where ω_m and ω_a are the mean and alternating component of the angular speed, as illustrated in Fig. 6, and f is the frequency of $\omega(t)$ and $\alpha(t)$.

The VAP angular velocity and acceleration are given by

$$\omega(t) = \omega_m + \frac{2\omega_a}{1-b} h_1(t)[1 - b\mathrm{e}^{(1-b/b)2h_2(t)-1}], \tag{18}$$

$$\alpha(t) = \frac{4f\omega_a}{1-b} K_1 \left[1 - (b + 2(1-b)h_2(t))\mathrm{e}^{(1-b/b)[2h_2(t)-1]}\right], \tag{19}$$

where the functions $h_1(t)$, $h_2(t)$, and K_1 are given by

$$h_1(t) = \begin{cases} 2ft - n_1 & \text{if } n_1 \text{ is even,} \\ n_1 - 2ft & \text{if } n_1 \text{ is odd,} \end{cases} \quad \text{where} \quad n_1 = \mathrm{int}\left(2ft + \frac{1}{2}\right), \tag{20}$$

$$h_2(t) = \begin{cases} 2ft - (n_2/2) & \text{if } n_2 \text{ is even,} \\ (n_2 + 1/2) - -2ft & \text{if } n_2 \text{ is odd,} \end{cases} \quad \text{where } n_2 = \mathrm{int}(4ft), \tag{21}$$

$$K_1 = \begin{cases} 1 & \text{if int}(2ft + 0.5) \text{ is even,} \\ -1 & \text{if int}(2ft + 0.5) \text{ is odd,} \end{cases} \tag{22}$$

where the function "int" rounds the argument down to the nearest integer. The VAP function depends on a smoothness parameter b. This can vary in the open interval (0, 1), in order to obtain $\omega(t)$ and $\alpha(t)$ curves of different smoothness and with different values of the maximum angular acceleration withstood by the brush shaft.

Curves ω and α against t of both functions are illustrated in Fig. 6. When $b \approx 0$, $\omega(t)$ is a triangle wave and $\alpha(t)$ is a square wave, so that the maximum angular acceleration is minimised. If $0 < b < \sim 4/9$, the maximum angular acceleration is smaller than its counterpart of the sinusoidal function, and both $\omega(t)$ and $\alpha(t)$ are smooth curves. If $\sim 4/9 < b < 1$, the maximum angular acceleration is greater than its counterpart of the sinusoidal function. Lastly, when $b \approx 1$, $\alpha(t)$ is a triangle wave and the maximum angular acceleration is maximised. It is noted that equating Eqs. (23) and (24) (presented below) gives $b \approx 4/9$. In general, b should be nearer to zero than to one, if small shaft accelerations are required. Lastly, it is important to mention that the VAP function is one way to obtain reduced shaft accelerations; other functions may enable to do so. However, the study of more functions of oscillation is out of the scope of this work.

From Eqs. (17) and (19), it can be shown that the maximum angular acceleration for the sinusoidal function is

$$\alpha_{\max} = 2\pi f \omega_a \tag{23}$$

and for the VAP function is

$$\alpha_{\max} = \frac{4 f \omega_a}{1-b}[1 - b e^{(b-1/b)}]. \tag{24}$$

The integral in Eq. (14) can now be solved for each function. By using Eq. (17), the integral in Eq. (14) for the sinusoidal function yields

$$h_i(t) = \frac{2\pi f r_A \omega_i \omega_a}{(2\pi f)^2 - \omega_i^2}(\cos 2\pi f t - \cos \omega_i t). \tag{25}$$

It may be easier to calculate numerically the integral for the VAP function. It can be demonstrated that Eq. (14) is approximately given by

$$h_i(t) = r_A \alpha(0) \sin \omega_i t \frac{t}{2n} + \sum_{j=1}^{n-1} \left\{ r_A \alpha\left(\frac{jt}{n}\right) \sin\left[\omega_i t \left(\frac{n-j}{n}\right)\right] \frac{t}{n} \right\}, \tag{26}$$

where the function $\alpha(0)$ ($\alpha(0) = \alpha_{\max}$, Eq. (24)) and $\alpha(jt/n)$ are obtained by substituting t by 0 and jt/n, respectively, in Eq. (19), and n is an integer number that should be large enough so as to obtain the required accuracy.

5. Analysis and validation of the model

5.1. Analysis

It is anticipated that in the results of this work, the first mode largely dominates the vibration characteristics of the bristle. Therefore, the tip tends to withstand the largest deflections, and the top the largest moments. Furthermore, as normally the tip is the part of the bristle that will become in contact with the road and debris, the deflection of the tip is of main interest. In view of these characteristics, this work will concentrate on the deflection of the tip and the bending moment (or stress) at the top.

As for the maximum stresses caused by the vibration of the bristle, they also tend to occur at the clamped end because the bristle is assumed prismatic and homogeneous. The moment M_z generates a linear distribution of stress, whose maximum value (tension or compression) is given by

$$S_{\max} = \frac{M_z(t_2/2)}{I_{zz}} = \frac{6M_z}{t_2^2 t_1}, \tag{27}$$

where t_1 and t_2 are the bristle breadth and width respectively, and they are indicated in Fig. 2. It is noted that this equation only includes the stresses due to the vibration in the weaker plane.

An analysis of Eqs. (11) and (15) shows that the deflection of the bristle tip, $y(l, t)$, and the bending moment at the clamped end, $M_z(0, t)$, as well as the stress, $S_{\max}(0, t)$, are independent of ω_m and are function of the terms ω_a, $\sin\phi$, r_A, b (or the type of function), f, l, and t. In addition, tip deflection depends on k_a (Eq. (10)), and the bending moment at the top on EI_{zz} and ρA. Both $y(l, t)$ and $M_z(0, t)$ are proportional to ω_a and have linear relationships with $\sin\phi$ and r_A. As $y(l, t)$ and $M_z(0, t)$ are proportional to ω_a, any value of ω_a can be selected, and the results can be extended to any other value. It is considered convenient to use $\omega_a = 1\,\mathrm{rad\,s^{-1}}$. In contrast, in a cutting brush $y(l, t)$ and $M_z(0, t)$ are function of the terms ω_a/ω_m, ${\omega_m}^2$, f, r_A, ϕ, l, EI_{zz}, ρA, and b [8]. The deflection and bending moment are not independent of ω_m, have linear relationships with r_A, and are proportional to ${\omega_m}^2$. The reason for the dependence on ω_m is that, as opposed to a flicking brush, the centrifugal forces in a cutting brush work in the weaker plane for bending deflections.

The variables that are investigated in this work are f, the type of function, b, l, ϕ, and r_A. The effects of the dimensions of the bristle cross-section, t_1 and t_2, and the material properties E and ρ are not studied here. It is expected that the behaviour of the bristle presents the same trends as those reported in the next section. However, different values of these parameters produce different values of the terms EI_{zz} and ρA and, therefore, of the natural frequencies (Eq. (16)). Unless otherwise stated, hereafter the bristles are of steel with $E = 207\,\mathrm{GPa}$, $\rho = 7800\,\mathrm{kg\,m^{-3}}$, $t_1 = 2\,\mathrm{mm}$, $t_2 = 0.5\,\mathrm{mm}$, and $l = 240\,\mathrm{mm}$. The geometrical parameters of the brush are $\phi = 26^\circ$ and $r_A = 112.5\,\mathrm{mm}$. All these values have been used in previous investigations [1,4–8]. For all the results $\omega_a = 1\,\mathrm{rad\,s^{-1}} = 9.55\,\mathrm{rev/min}$, and for the validation of the model $\omega_m = 60\,\mathrm{rev/min}$. The range of frequency $1\,\mathrm{Hz} \leqslant f \leqslant 50\,\mathrm{Hz}$ is selected, taking into account practical considerations for achieving f, and because this range contains the first and second natural frequency of the bristle. The effect of bristle wear is dealt with by analysing the range of bristle length $140\,\mathrm{mm} \leqslant l \leqslant 240\,\mathrm{mm}$. For the mount radius, the range investigated is $0 < r_A \leqslant 200\,\mathrm{mm}$. For b and ϕ, results are reported for the full ranges $0 < b < 1$ and $0 \leqslant \phi \leqslant 90^\circ$ $(0 \leqslant \sin\phi \leqslant 1)$.

The following decisions are made: the time interval [0, 1 s] is chosen to track the maximum values of $y(l, t)$ and $S_{\max}(0, t)$. This is considered appropriate, as it provides a useful insight into the behaviour of the brush and because the bristles of a constrained gutter brush are not normally in free flight during more than a second. Besides, internal damping would tend to affect significantly the results if very long periods of time were analysed. A time interval, i.e., the difference between two consecutive time values used to determine $y(l, t)$ and $S_{\max}(0, t)$, of at most 2 ms is selected. Additionally, values of y and $S_{\max}$ are calculated for frequency increments of 0.1 Hz. Lastly, the results are based on the first four modes of vibration, and $n \geqslant 2000$ (Eq. (26)) for the VAP function. These decisions are based on the results of sensitivity analyses performed for the case of a cutting brush [8].

5.2. Validation

The validation of the model is carried out by using several Finite Element Models (FEMs). Firstly, a small-deflection FEM built in ANSYS® is used to verify the correctness of the model. The element is a 3-D quadratic beam with mid-side node (BEAM189), which includes shear-deformation effects and stress-stiffness terms. The bristle is modelled with at least 50 elements (101 nodes). An inertia load (DOMEGA) equivalent to $\rho A a_t$ is applied. However, the loading curve is approximated by at least 100 straight lines per cycle. The integration time step was 0.02 ms or smaller. All the other data is as described in Section 5.1. The results of several analyses carried out with different numbers of nodes and time steps indicate that the errors associated with the values above are negligible in comparison with the differences obtained between the analytical and the FEM. Secondly, a large-deflection FEM is utilised to study the validity of the assumption of small deflection. Thirdly, the effect of damping is also investigated. Rayleigh damping is assumed, and the damping coefficients were obtained experimentally. Constant values of $0.104\,\mathrm{s^{-1}}$ for the mass matrix multiplier and $1.07 \times 10^{-5}\,\mathrm{s}$ for the stiffness matrix multiplier were obtained. Finally, a FEM is used to study the behaviour of the bristles when they are subjected to the 3-D deformations produced by all the inertia forces, i.e., the centrifugal forces and those produced by the angular acceleration of the brush and Coriolis accelerations. Damping and large deflection are also considered in this model. A short summary of the results obtained from these FEMs is presented herein.

Regarding the small-deflection FEM, the maximum relative differences between the models are 0.6% for the bending moment and 0.3% for the deflection, from all the results obtained. The differences are calculated as the ratio between the maximum difference in the deflection or bending moment and the maximum deflection or bending moment in the time range reported. A detailed analysis indicates that these differences are mainly due the limited number of modes taken into account by the analytical models. Thus, the results suggest that the analytical model derived is valid. Fig. 7 shows an example in which the analytical model and the FEM are compared. Similarly, the results of the FEM that considers large deflection indicate that the differences (calculated as described above) between the FEM and the analytical model are very small but can reach about 1% when the frequency is near a natural frequency or an odd fraction of it. For other frequencies, the differences are estimated to be less than about 0.2% for both deflection and moment. As for the effect of damping, the maximum differences encountered between the FEM with damping and the analytical model are about 3% near the natural frequencies or odd fractions of them. However, far from these frequencies, the differences are about 0.6% or smaller. This is because for frequencies near odd fractions of the natural frequencies the maximum deflection and moment tend to occur at the end of the time range studied. Fig. 8 provides an example that compares the tip deflections from the analytical model and the FEM that considers large deflection and damping.

The results of the FEM that considers 3-D deformations, damping, and large deflection suggest that the deflections in the stronger plane are generally much smaller than those in the weaker plane, reaching a maximum value of about 1 mm. This validates the assumption that, due to the aspect ratio of the cross-section of the bristle, this deflects mainly in the weaker plane. The analyses also indicate that twisting is very small, reaching a maximum value of the order of 0.4° (0.007 rad). It is estimated that for frequencies smaller than the first natural frequency in the stronger plane, $f_{1s} = 28.89$ Hz, the errors of the results reported in the present work lie within 4%. For this frequency and higher ones, the errors may reach values of about 8%. For instance, the differences in the maximum deflection and stress when $f = f_{1s}$ are 3% and 8%, respectively (Fig. 9). As a high accuracy is not a main concern in this work, the estimated errors above indicate that the

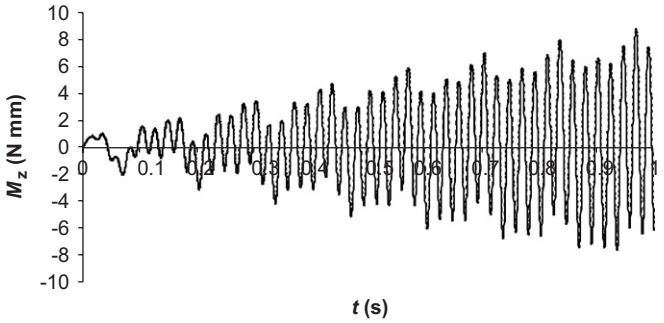

Fig. 7. Bending moment at the bristle top against time. VAP function with $f = 15$ Hz and $b = 0.05$. — FEM, –·– analytical model.

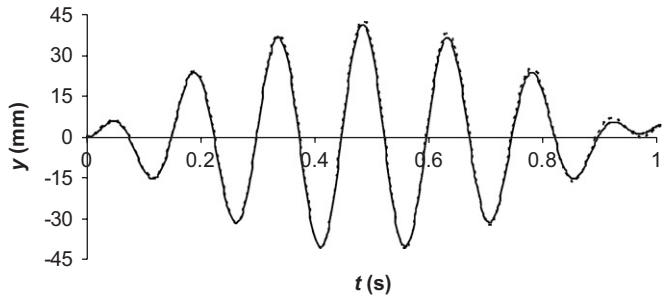

Fig. 8. Bristle tip deflection against time. Sinusoidal function with $f = 6.2$ Hz. — FEM that considers large deflection and damping, –·– analytical model.

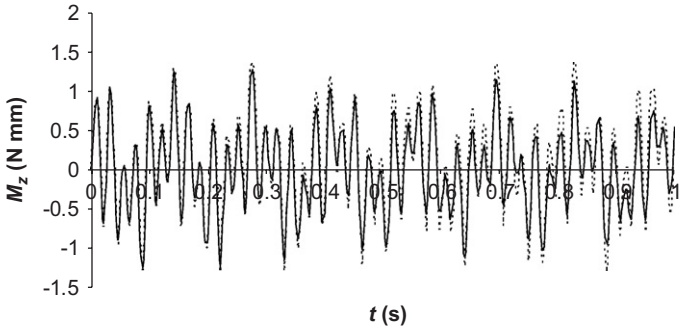

Fig. 9. Bending moment at the top against time. VAP function with $f = f_{1s} = 28.89$ Hz and $b = 0.06$. — FEM that considers 3-D deformations, large deflection and damping, –·– analytical model.

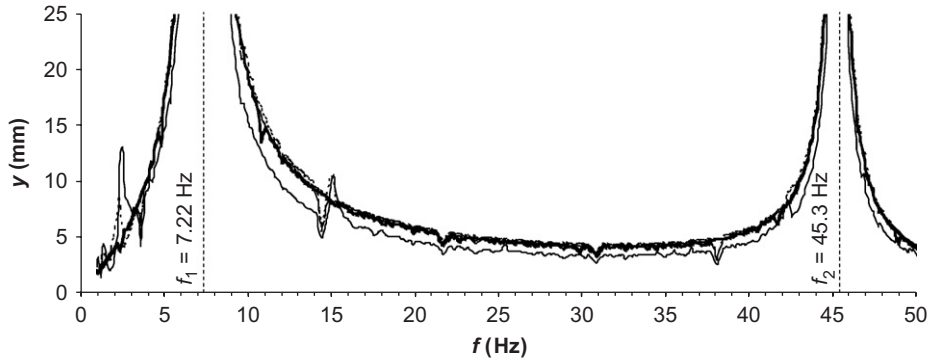

Fig. 10. Maximum deflection of the bristle tip against frequency. sinusoidal, — $b = 0.01$, –·– $b = 0.5$, ---- $b \approx 1$.

model provides a useful insight into the behaviour of the bristles. It is noted that these results are based on a mean rotational speed of 60 rev/min. Due to the centrifugal forces, higher rotational speeds will tend to produce higher deflections in the stronger plane, which will tend to affect more the vibrations in the weaker plane.

In addition to the analyses reported above, other analyses were carried out. Regarding the effect of shearing deformations and rotary inertia, the literature (e.g., Ref. [17]) and some analyses performed indicate that these are insignificant for this case, as the bristle is an extremely slender beam. Axial vibrations are also negligible because of the characteristics of the system and the high natural frequencies for longitudinal vibrations (these are greater than 10 730 Hz for the cases reported in this article).

6. Results and discussion

6.1. Brush oscillation frequency

The effects of the frequency of oscillation of the brush, f, for different oscillatory functions are illustrated in Figs. 10 and 11. These present the maximum deflection of the bristle tip and maximum stress, respectively, against frequency, in the time interval [0, 1 s]. As the stress is proportional to the bending moment (Eq. (27)), it is not necessary to consider the latter here. For reasons that will be discussed in Section 6.2, the curves for the sinusoidal function and the VAP function with $b = 0.5$ are rather coincident. As expected, for all the functions of oscillation, resonance tends to occur when the frequency is close to the first or the second natural frequency ($f_1 = 7.22$ and $f_2 = 45.3$ Hz, from Eq. (16)). Notably, the results indicate that a peculiar behaviour, a condition similar to resonance, tends to occur for the VAP function when the frequency is near an odd fraction of any of the first four natural frequencies (only the first four modes were considered). This condition is accentuated for

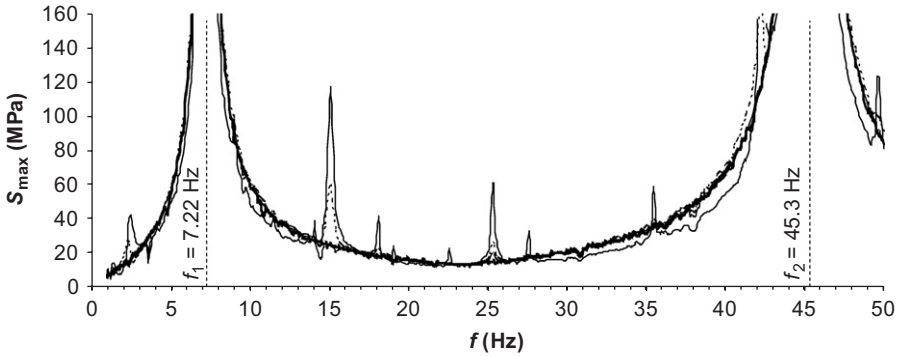

Fig. 11. Maximum stress at the bristle top against frequency. sinusoidal, — $b = 0.01$, –·– $b = 0.5$, ---- $b \approx 1$.

Table 1
Frequencies in Hz at which there is a noticeable peak in the maximum stress and/or deflection

Mode	$f_i/1$	$f_i/3$	$f_i/5$	$f_i/7$	$f_i/9$	$f_i/11$
1	7.22	2.41	1.44	1.03		
2	45.3	15.1	9.05			
3		42.3	25.4	18.1	14.1	
4			49.7	35.5	27.6	22.6

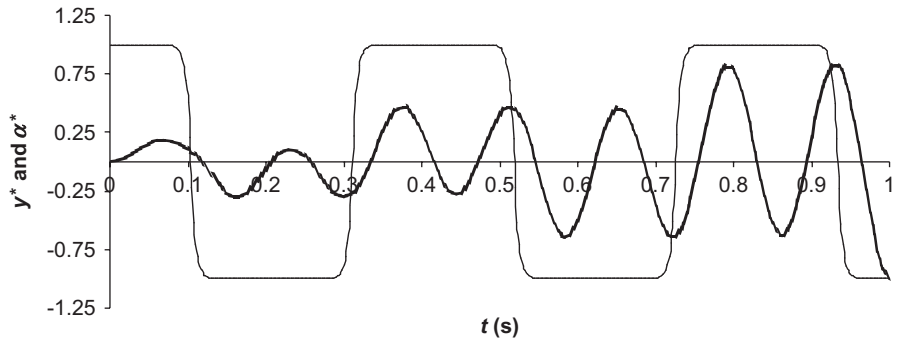

Fig. 12. Normalised bristle tip deflection, y^*, and angular acceleration, α^*, against time. $b = 0.05$ and $f = f_1/3 = 2.41$ Hz. y^*, — α^*.

$b = 0.01$. It is of interest to mention that $b = 0.01$ provides almost the same results as $b \approx 0$; the former value has been selected here because smaller values tend to require much larger values of n in Eq. (26) for a given accuracy. Some of the values of frequency at which peaks can be observed in the deflection and/or the stress curves are presented in Table 1. It is also noted that more peaks become noticeable when longer times are analysed. An analysis of this table and Figs. 10 and 11 indicates that for any of the four modes (i.e., for any row), the lower the frequency, the shorter the peak, for reasons discussed in the next paragraph.

The reason for the occurrence of high vibration amplitudes and stresses at odd fractions of the natural frequencies, when b is close to zero, may be observed in Figs. 12 and 13, in which $f = f_1/3 = 7.22/3 = 2.41$ and $f = f_1/5 = 1.44$ Hz, respectively. Fig. 12 presents curves of normalised values of the deflection of the tip, y^*, and the angular acceleration, α^*, and Fig. 13 shows curves of a normalised maximum stress, S^*, and angular acceleration, α^*. A normalised value corresponds to the ratio between the deflection, stress, or angular acceleration and its maximum absolute value in the time interval shown. In these cases, as the bristle oscillates, the abrupt change in angular acceleration tends to coincide with the maximum (or minimum) bristle

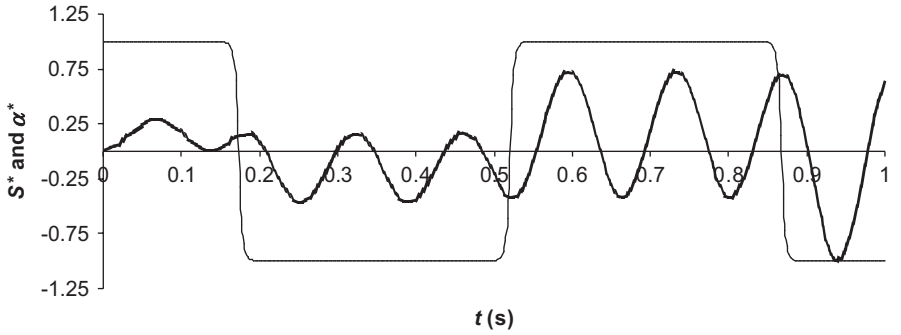

Fig. 13. Normalised maximum stress, S^*, and angular acceleration, α^*, against time. $b = 0.02$ and $f = f_1/5 = 1.44$ Hz. ▪▪▪▪▪▪▪▪ S^*, — α^*.

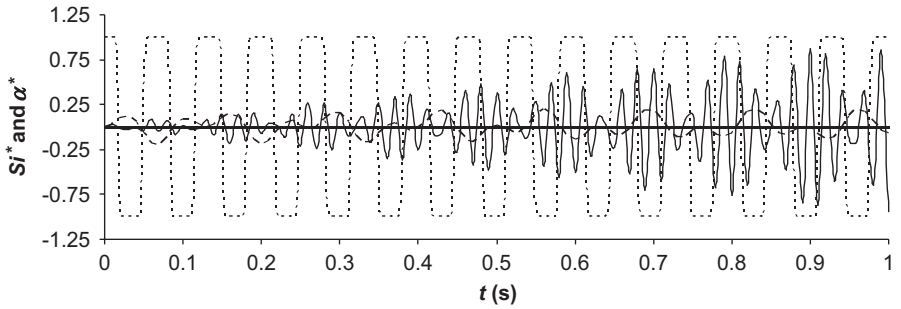

Fig. 14. Normalised stresses S_1^*, S_2^*, and S_3^*, at the clamped end and angular acceleration, α^*, against time. $b = 0.05$ and $f = f_2/3 = 15.1$ Hz. —·— S_1^*, — S_2^*, ▪▪▪▪▪▪▪▪ S_3^*, - - - - α^*.

deflection. The directions of the deflection and angular acceleration are such that each time the latter changes direction, the bristle tends to increase its maximum deflection. The deflection amplitude remains practically constant up to the next change in angular acceleration, where the amplitude increases again. This behaviour can also be explained by considering the work of the inertia force produced by the angular acceleration. For example, from Fig. 12, it can be concluded that this force does positive work about two-thirds of the time, when the force and the velocity of the bristle have the same direction. In the remaining time, the work of the force is negative. Therefore, there is a net positive work that produces increased vibration amplitudes. Similarly, in the case of Fig. 13, the force does positive work about three-fifths of the time and negative work about two-fifths. Finally, as indicated in the previous paragraph, the results indicate that the lower the odd fraction of the frequency, the slower the process of increasing deflection; this may be inferred from Figs. 12, 13, and 10 or 11.

A similar behaviour is observed for other odd fractions of the natural frequencies. Fig. 14 provides an example of this phenomenon when $f = f_2/3 = 15.1$ Hz. The stresses due to the first three modes are separated, and they are normalised with respect to the overall maximum stress in the time interval shown. It may be observed that the first mode has a rather constant effect along the time line, i.e., amplitudes are not increasing, and that the third mode has a negligible effect. In contrast, the second mode is becoming dominant as time passes, as $f = f_2/3$, and a condition similar to resonance is achieved (a beating phenomenon is observed, and each beat has higher amplitudes than those of the preceding one). The abrupt changes in the angular acceleration and maximum tip deflections due to the effect of the second mode tend to occur simultaneously and in the "appropriate" direction.

On the other hand, downwards peaks can be observed in Figs. 10 and 11, indicating that the VAP function with certain frequencies tends to reduce bristle oscillations when they are compared with those produced near these frequencies. From a more detailed analysis around those peaks, it is found that for $f = f_1/2 = 3.61$ and $f = 2f_1 = 14.4$ Hz, the oscillations and stresses tend to be lower than those generated around these frequencies.

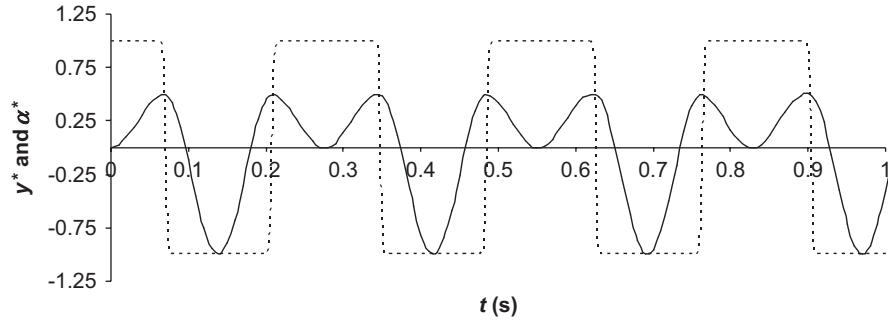

Fig. 15. Normalised tip deflection, y^*, and angular acceleration, α^*, against time. $b = 0.02$ and $f = 3.61\,\text{Hz} = f_1/2$. — y^*, ---- α^*.

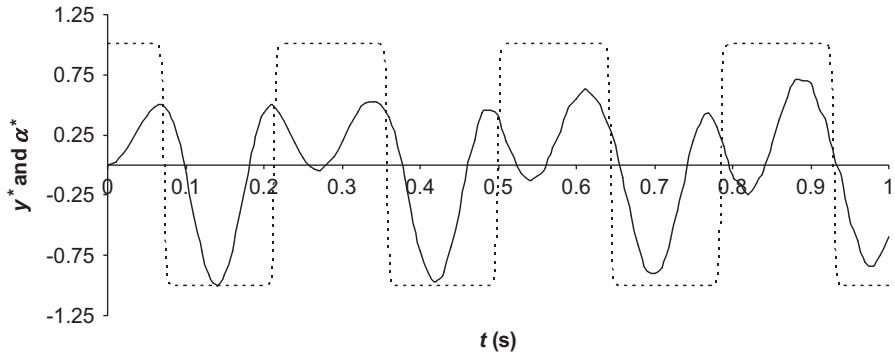

Fig. 16. Normalised tip deflection, y^*, and angular acceleration, α^*, against time. $b = 0.02$ and $f = 3.5\,\text{Hz}$. — y^*, ---- α^*.

The reason for this behaviour may be observed in Figs. 15 and 16, in which $f = 3.61\,\text{Hz} = f_1/2$ and $f = 3.5\,\text{Hz}$, respectively. When $f = 3.61\,\text{Hz}$, it can be noticed that the changes in the angular acceleration coincide with a maximum deflection (and also bending moment or stress), in such a way that the positive deflections are maintained small. This does not occur when $f = 3.5\,\text{Hz}$. A similar phenomenon is observed when $f = 2f_1$.

From Figs. 10 and 11, it can also be noted that the stress is more sensitive to the changes in frequency than the deflection when f is greater than f_1. For example, whereas the maximum stress has a peak at about $f_3/5 = 25.4\,\text{Hz}$, a peak in the maximum deflection is not clearly noticed. It is observed that the deflection is mainly influenced by odd fractions of the fundamental frequency, whereas odd fractions of the natural frequencies of higher modes have a profound effect on bristle stresses. This may be explained, in part, by the fact that in the results reported in this work, higher frequencies tend to produce smaller deflections but slopes comparable with those of lower frequencies.

6.2. Smoothness parameter

As the VAP function has been devised to obtain small shaft accelerations, the discussion in Section 6.1 concentrated mainly on small values of the smoothness parameter, b. This section extends this study, investigating the whole interval $0 < b < 1$. When the frequency of brush oscillation is close to the first or second natural frequency, the larger the value of b, the higher the maximum deflection and stress. This is indicated by the examples in Figs. 17 and 18. The same behaviour tends to occur for frequencies far from odd fractions of the natural frequencies, as shown by the examples in Fig. 19 (curves for $f = 1.2$ and $40\,\text{Hz}$), and as may be inferred from the curves for $b = 0.01$ and $b \approx 1$ in Figs. 10 and 11. The reason for this can be explained by considering again the work of the inertia force produced by the angular acceleration. Increasing b raises the maximum angular acceleration developed, as shown in Fig. 20. At $t = 0$, the greater angular acceleration when b is larger creates higher inertia forces and, consequently, produces greater work, deflections, and velocities (Fig. 21). Higher velocities imply larger displacements in a given time interval, enhancing the work of the

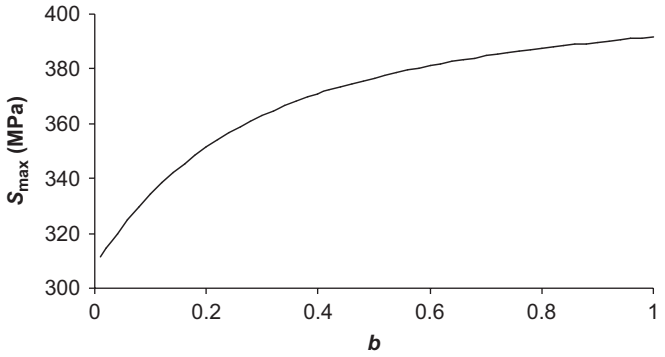

Fig. 17. Maximum stress against b for $f = 7$ Hz.

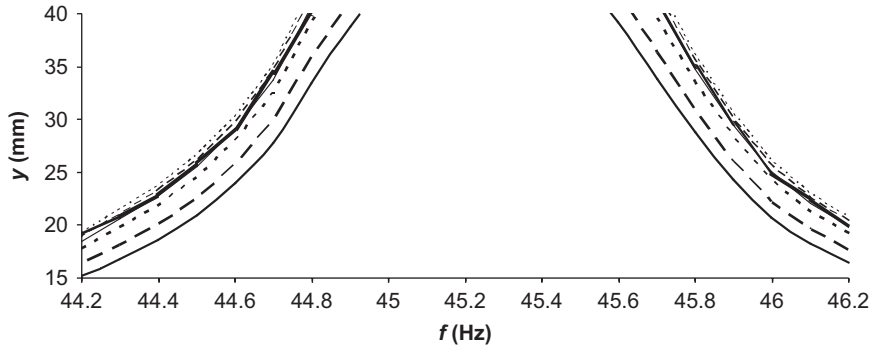

Fig. 18. Maximum tip deflection against frequency. sinusoidal, $b = 0.01$, $b = 0.1$, $b \approx 0.3$. $b = 0.5$, $b = 0.7$, $b \approx 1$.

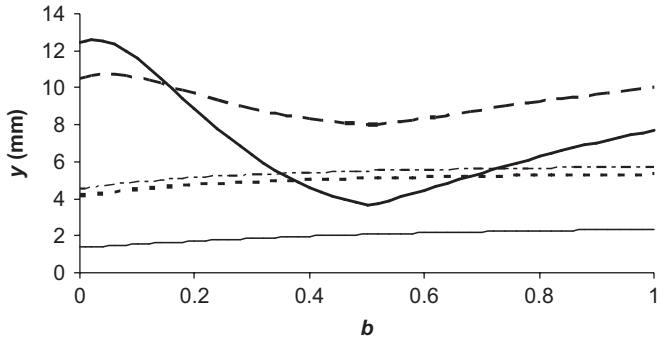

Fig. 19. Maximum tip deflection against b for a set of frequencies. $f = 1.2$ Hz, $f = 40$ Hz, $f = f_1/3 = 2.41$ Hz, $f = f_2/3 = 15.1$ Hz, $f = f_4/11 = 22.6$ Hz.

inertia force. The results indicate that this effect compensates for the reduced magnitude of $\alpha(t)$ when this is approaching zero or is increasing from zero. The vibrations for longer times exhibit these characteristics. Thus, the bristle tends to withstand greater deflection and stress amplitudes for larger values of b.

Bristle dynamics for brush frequencies near odd fractions of the natural frequencies may also exhibit a monotonic increase of maximum deflection or stress with b (e.g., curve for $f = f_4/11 = 22.6$ Hz in Fig. 19). However, a second trend is observed. With increasing b in the interval (0, 1), the maximum deflections and stresses may or may not first increase slightly; then they decrease up to a minimum and rise again. Fig. 19

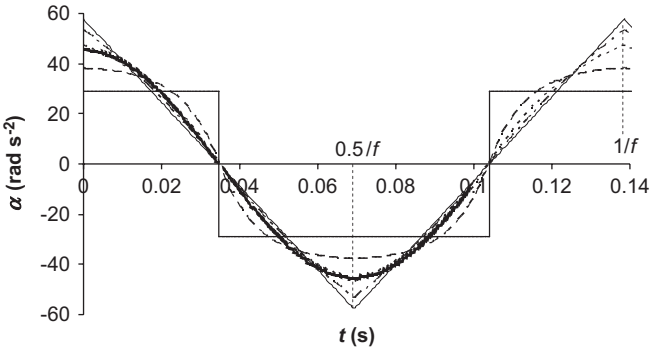

Fig. 20. Angular acceleration against time when $f = 7.22$ Hz. ▪▪▪▪▪▪▪▪ sinusoidal, — $b \approx 0$, – – – · $b = 0.25$, - - - - $b = 0.5$. – · – · – · $b = 0.75$, — $b \approx 1$.

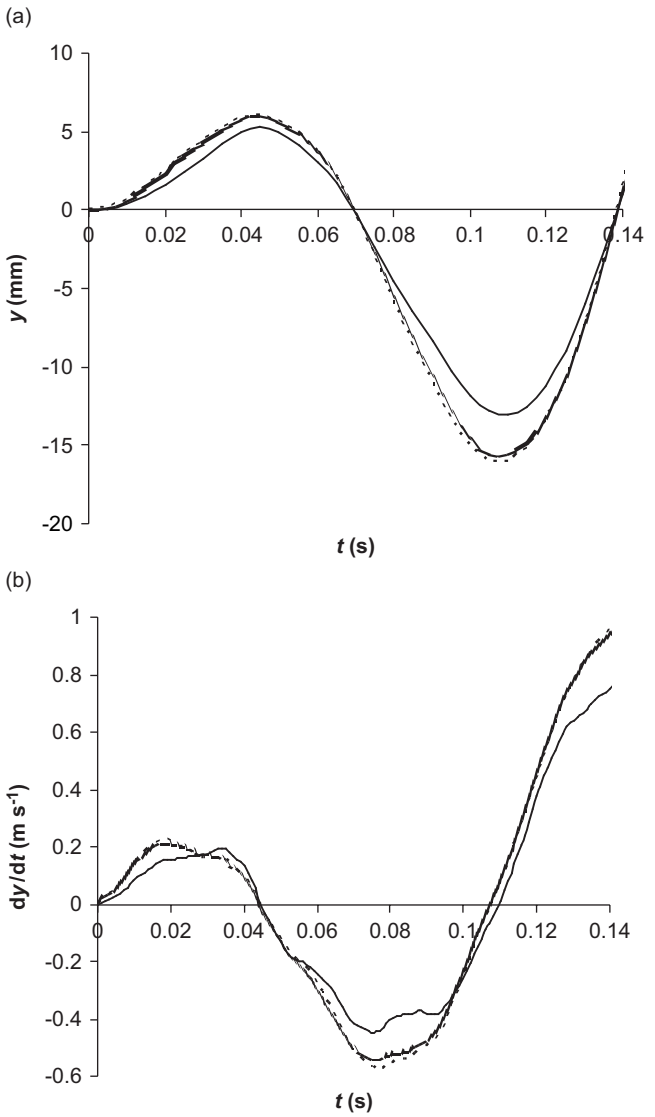

Fig. 21. Tip deflection and velocity against time when $f = 7.22$ Hz: (a) tip deflection, (b) tip velocity. ▪▪▪▪▪▪▪▪ sinusoidal, — $b = 0.01$, - - - - $b \approx 1$.

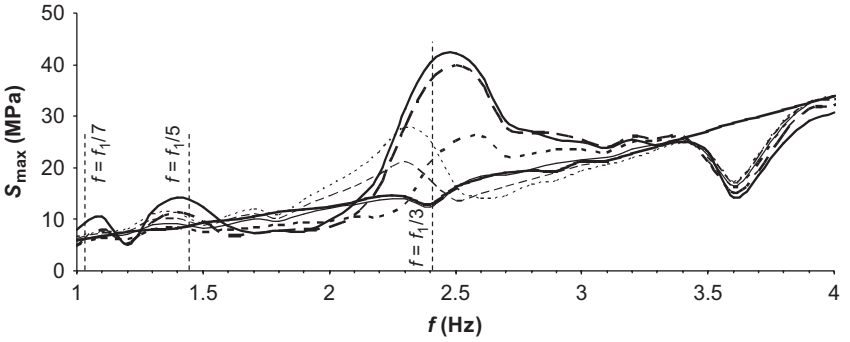

Fig. 22. Maximum top stress against frequency. sinusoidal, $b = 0.01$, $b = 0.1$, $b \approx 0.3$, $b = 0.5$, $b = 0.7$, $b \approx 1$.

($f = f_1/3 = 2.41$ and $f = f_2/3 = 15.1$ Hz) and Fig. 22 show some examples of this trend. In Fig. 19, for $f = 2.41$ and 15.1 Hz, the maximum deflection occurs when $b \approx 0.02$ and 0.05, respectively, and the minimum deflection when $b \approx 0.5$ and 0.51, respectively. At least for the frequencies in Table 1, excepting the natural frequencies, analyses suggest that maximum tip deflections and top stresses tend to be minimum when b is roughly in the intervals (0, 0.5) and (0.25, 0.5), respectively. The value of b that minimises y or S_{max} tends to be near 0.5 for larger odd fractions of the natural frequencies. The next paragraphs discuss these findings.

The first trend, i.e., maximum deflections or stresses rise with increasing b, normally occurs when the resonant effect of the odd fraction of the natural frequency is weak. This tends to take place mainly for the deflection when the frequency is near f_1 or f_2 (e.g., when $f = f_2/5 = 9.05$ Hz, which is near $f_1 = 7.22$ Hz) and for small odd fractions of f_3 and f_4 (e.g., $f_3/7$ or $f_4/7$ or smaller values). In contrast, the effect of the third and fourth modes on the top stress is, in general, much higher than that on the deflection. Consequently, the stress mostly follows the second trend. As discussed in Section 6.1, the condition similar to resonance that occurs for small values of the smoothness parameter is due to the plateau of the angular acceleration curve. As b is increased from zero, the plateau and, consequently, the resonant phenomenon, diminish gradually up to about $b \approx 0.5$. At this value of b, this phenomenon is weak or cannot be easily noticed. When $b = 0.5$, the VAP angular acceleration fairly resembles its sinusoidal counterpart, as shown in Fig. 20. However, there is not a value of b for which the VAP function corresponds closely to the sinusoidal function. As the resonant behaviour at odd fractions of the natural frequencies reduces with increasing b in the interval (0, ~0.5], the maximum deflection and stress tend to decrease. The slight increase of deflections and stresses with b near $b = 0$ (e.g., curves for $f = 2.4$ and 15.1 Hz in Fig. 19) seems to be due to the increased magnitude of the maximum angular acceleration. This increases tip deflections and velocities, with the subsequent increase in the work done by the inertia force. However, when longer times are analysed, the resonant behaviour becomes dominant and compensates for the smaller magnitude of b. Therefore, this slight increase of y and/or S_{max} becomes less noticeable when longer times are studied. It also tends to disappear for smaller odd fractions of the natural frequencies, because the resonant behaviour acts more slowly, as stated in Section 6.1.

When b increases in the interval [~0.5, 1), the maximum deflections and stresses tend to increase. An analysis of the dynamics of the bristle indicates that there is also a condition similar to resonance in this range. As occurs in the case of a small value of b, for values of b in the interval above, it is observed that when f is an odd fraction of f_i ($i = 1$–4), the ith mode is the one that exhibits the resonant behaviour. Some examples of this phenomenon are presented in Figs. 23–25. Fig. 23 presents the deflection of the tip and the angular acceleration curves for the sinusoidal function and the VAP with $b \approx 1$, when $f = f_1/3 = 2.41$ Hz. For convenience, a longer time interval is shown, and y and α have not been normalised so that a direct comparison of the curves can be made. For the sinusoidal function, the amplitude of vibration does not increase. In contrast, for the VAP function, the amplitudes of vibration increase with every cycle of the angular acceleration. Due to the triangular shape of the VAP function with $b \approx 1$, the deflection becomes slightly ahead when compared to its counterpart of the sinusoidal function. This enables the VAP function to produce, every angular acceleration cycle, a net positive work that increases vibration amplitudes with time.

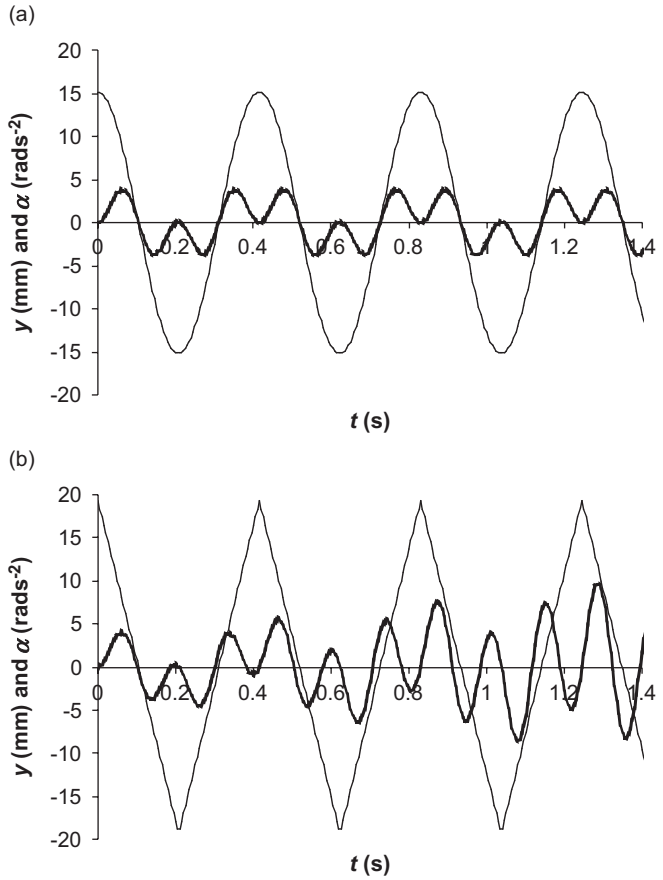

Fig. 23. Tip deflection and angular acceleration against time for $f = f_1/3 = 2.41$ Hz: (a) sinusoidal function, (b) VAP function with $b \approx 1$. ⠿⠿⠿⠿⠿ y, — α.

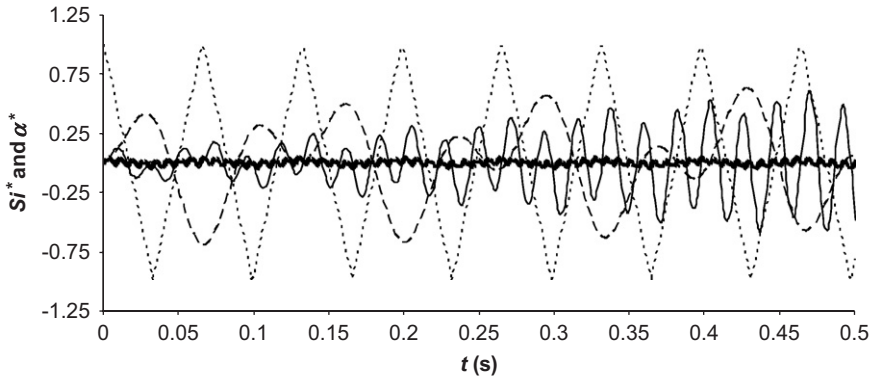

Fig. 24. Normalised stresses S_1*, S_2*, and S_3*, at the clamped end and angular acceleration, α*, against time. VAP function with $b \approx 1$ and $f = f_2/3 = 15.1$ Hz. – –. S_1*, — S_2*, ⠿⠿⠿⠿⠿ S_3*, - - - - α*.

This resonant behaviour is strongest when $b \approx 1$, i.e., when $\alpha(t)$ becomes a triangular wave. As b is reduced from 1 to about 0.5, the shape of $\alpha(t)$ becomes similar to the sinusoidal function, the resonant behaviour weakens, and the response of the bristle becomes practically the same (at least for not so long times) as that when the sinusoidal wave is applied. In the example in Fig. 24, the stresses due to the first three modes are separated, and they are normalised with respect to the overall maximum stress in the time interval shown; the

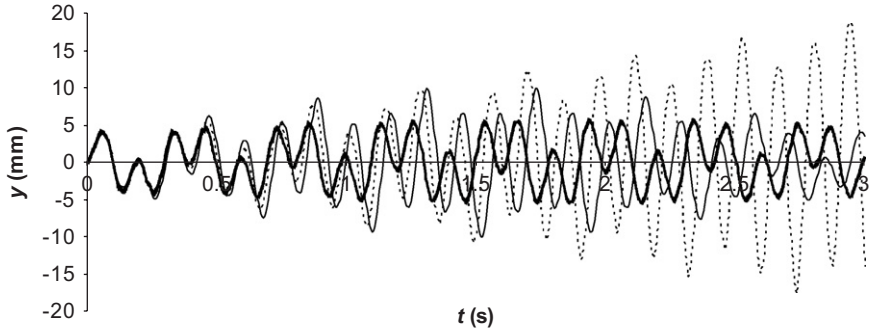

Fig. 25. Tip deflection against time for the VAP function with $b \approx 1$. — $f = 2.3$ Hz, ---- $f = f_1/3 = 2.41$ Hz, ▪▪▪▪▪▪▪▪ $f = 2.5$ Hz.

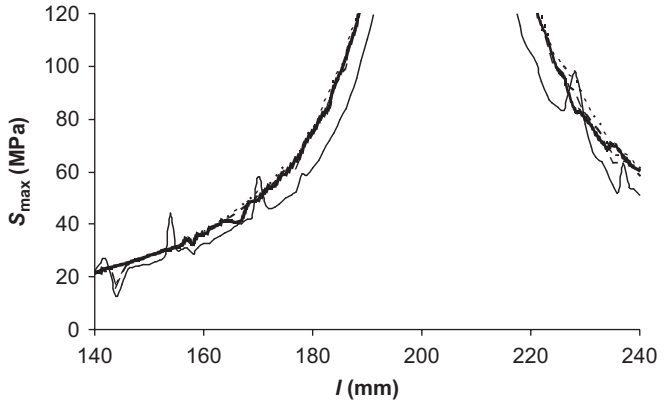

Fig. 26. Maximum stress at the bristle clamped end against bristle length when $f = 10$ Hz. ▪▪▪▪▪▪▪▪ sinusoidal,— $b = 0.01$, –·– $b = 0.5$, ---- $b \approx 1$.

effect of the fourth mode is very small and is not shown. The second mode becomes dominant with time as $f = f_2/3$. Finally, Fig. 25 presents curves for the deflection against time for the VAP function with $b \approx 1$ and three different frequencies: 2.3 Hz, $f_1/3 = 2.41$ Hz, and 2.5 Hz. This figure uses a longer time interval [0, 3 s], and it is presented to explain the fact that the peaks in Fig. 22 do not occur exactly at $f_1/7$, $f_1/5$, and $f_1/3$. Although, for example, the maximum deflection for $f_1 = 2.3$ Hz in the interval [0, 1 s] is greater that its counterpart for $f_1 = 2.41$ Hz, the resonant behaviour is exhibited for $f = f_1/3 = 2.41$ Hz but not for the other two frequencies. When longer times are analysed, the peaks tend to fall more exactly at odd fractions of the natural frequencies. An analysis for all the other odd fractions of the natural frequencies in Table 1 indicates that a similar behaviour is present.

6.3. Bristle wear

As the natural frequencies of the bristle depend on its length (Eq. (16)), bristle wear (reduction of its length) has the effect of modifying its natural frequencies, and, therefore, the plot of deflection or stress against bristle length presents similar peaks to those in Figs. 10 and 11. As an example, Fig. 26 presents the maximum stresses for $f = 10$ Hz. As from Eq. (16), $f_1 = 10$ Hz for $l = 204$ mm, the deflections and stresses become high around this length. Other peaks occur at about $l = 237$, 228, 170, and 154 mm, as $f_{3(l=237.0\,\mathrm{mm})}/13 = 10$ Hz, $f_{2(l=228.4\,\mathrm{mm})}/5 = 10$ Hz, $f_{2(l=170.2\,\mathrm{mm})}/9 = 10$ Hz, and $f_{2(l=154.0\,\mathrm{mm})}/11 = 10$ Hz. In addition, the curves for the VAP function exhibit a downwards peak at about $l = 144$ mm, as $f_{1(l=144.2\,\mathrm{mm})}/2 = 10$ Hz. This is in agreement with the findings discussed in Section 6.1.

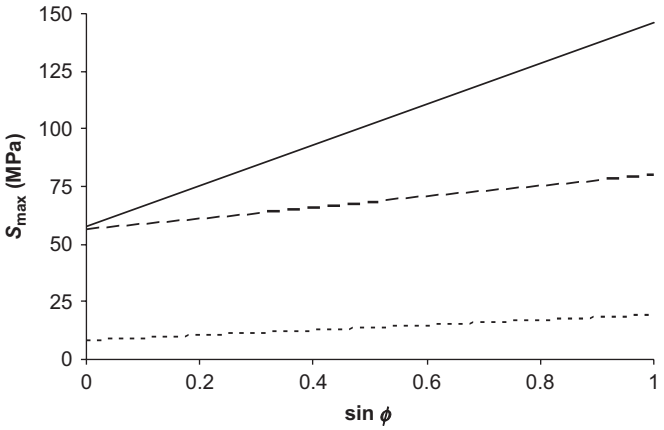

Fig. 27. Maximum stress against $\sin\phi$ for a set of frequency and function combinations. — $f = 6$ Hz, $b = 0.1$; – – · $f = 40$ Hz, sinusoidal; - - - - $f = 2$ Hz, sinusoidal.

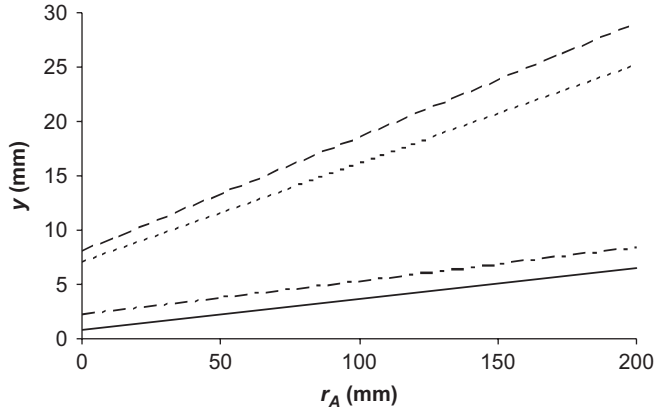

Fig. 28. Maximum tip deflection against mount radius for the sinusoidal function and a set of frequencies. — $f = 50$ Hz, – · – $f = 20$ Hz, – – · $f = 10$ Hz, - - - - $f = 5$ Hz.

6.4. Bristle mount angle and mount radius

The preceding results were obtained for a mount angle $\phi = 26^\circ$ and a mount radius $r_A = 112.5$ mm. However, as the relationships between $y(l, t)$ or $M_z(0, t)$ and both $\sin\phi$ and r_A are linear, as stated in Section 5, they can be extended to any other pair of values. Figs. 27 and 28 provide some examples, and they indicate that the maximum stress and deflection increase with ϕ and r_A. This is because the larger the mount angle and mount radius, the larger the tangential accelerations withstood by the bristle, as demonstrated by the second part of Eq. (7). The lines exhibit various slopes and various intercepts with the axes $r_A = 0$ and $\sin\phi = 0$, because of the different responses of the bristle for different functions and frequencies.

6.5. Additional remarks

The behaviour of an oscillatory, freely rotating flicking brush is very complex. The parameters of the oscillatory function (f, ω_a, and function type, including the value of b if applicable) have a profound effect on bristle dynamics. Small changes in, for instance, the frequency of oscillation, the shape of $\omega(t)$, and the length of the bristle may alter dramatically the response of the system. As the VAP function tends to produce a more variable response than that of the sinusoidal function, it could be used to alter brush behaviour. For example, the amplitudes of bristle oscillation may be enhanced or reduced by the manipulation of the frequency. It has

to be taken into account that larger deflections and higher mode vibrations may induce higher stresses, which may shorten the fatigue life of the bristles.

Even though a gutter brush works in contact with the road, it might be raised from the surface during some periods. Therefore, it may be necessary to interrupt brush rotation or its oscillations or to avoid a frequency that produces a resonant behaviour. This is particularly important for the function derived by the authors, which tends to produce large vibration amplitudes and stresses at various frequencies of oscillation of the brush. Moreover, the characteristics of a constrained brush are also affected by its free-flight behaviour. This is because gutter brushes normally work tilted, and a fraction of the bristles are in free flight at a given time. Henceforth, it is necessary to consider the dynamics of the bristles that are in free rotation, because of bristle stresses and due to the manner in which they come in contact with the road surface and debris. This initial contact may play an important role in sweeping performance, as it has been shown that the way in which the bristles impact the road affects brushing forces [4]. It is considered that this work has provided a useful insight into the free flight dynamics of the brush, and it constitutes a starting point for analysing the behaviour of a constrained brush. Consequently, this work does not aim at determining an optimum oscillatory function, value of the smoothness parameter, or frequency for improved sweeping, but rather at investigating its effect on bristle dynamics. For the bristles in contact with the road surface in a working brush, a particular oscillatory function or value of b may be beneficial, and there may be some frequencies with which improved sweeping performance is obtained. From the knowledge of the behaviour of a constrained brush and that of a free-rotating brush, a combination of frequencies that produces acceptable behaviour of both bristles in free flight and constrained ones may be determined. However, more research is needed to study brush-surface/debris interaction.

The literature review shows that brush oscillations affect the coefficient of friction and brushing efficiency. This is partly due to the high-frequency vibrations and impact forces that may be developed. In addition, as mentioned before, the oscillation may produce higher bristle stresses, affecting bristle life, which should be dictated by wear rather than fatigue. More research has to be carried out to determine whether these oscillations may be tuned to achieve certain patterns of motion of the bristle tips and to affect the coefficient of friction so that sweeping performance can be improved. If so, brush setup may be automatically controlled for different types of debris and working conditions in order to increase efficiency. Other potential application in which brush oscillations may improve performance is in the case of industrial cleaning, where very soiled surfaces are commonly found.

Last but not least, the model developed and the results that have been presented in this section may be readily adapted to the case of a cantilever beam that is subjected to 2-D small transverse vibrations, when a sinusoidal or a VAP wave is applied. This article demonstrated that the VAP function is capable of generating a condition similar to resonance when the frequency is an odd fraction of the natural frequency of the beam. Therefore, small changes in the frequency and the shape of the VAP wave by means of the smoothness parameter may be utilised in the hypothetical case in which a cantilever beam has to be excited towards resonance. Moreover, as the VAP function is able to excite a particular mode by means of a frequency equal to an odd fraction of the natural frequency of that mode, small frequencies may be required. This may be especially useful to excite high-frequency modes without the need for producing a high frequency disturbing force.

7. Conclusions

An analytical model for the dynamics of a novel oscillatory, freely rotating flicking brush for road sweeping was developed. The bristles were treated as cantilever beams subjected to small deflections, and two functions of oscillation of the brush angular speed were studied: a sinusoidal function and a novel function derived by the authors to produce small shaft accelerations. The latter function depends on a smoothness parameter, b, which can be varied from $b \approx 0$, when the angular acceleration becomes a square wave and its maximum value is minimised, to $b \approx 1$, when it becomes a triangle wave. The variables that affect brush dynamics were identified. According to the model and the results, brush dynamics is highly influenced by the type of function, the smoothness parameter, the frequency of oscillation, and the dimensions (t_1, t_2, l), density, and Young's modulus of the bristle. Additionally, bristle deflections and stresses are proportional to the alternating

component of the angular speed, are independent of the mean component, and have a linear relationship with the sine of the mount angle and the mount radius. The model was applied to study the dynamics of the bristle under different frequencies and functions of oscillation, bristle lengths, mount angles, mount radii, and different values of the smoothness parameter, b. It was shown that resonance tends to occur when the frequency of oscillation of the brush is near the first or second natural frequency, regardless of the type of function from those studied. Moreover, it has been found that for the VAP function, a condition similar to resonance tends to occur at odd fractions of, at least, the first four natural frequencies. This phenomenon tends to be accentuated as b approaches 0 or 1 and weakens towards $b \approx 0.5$, where the VAP angular acceleration fairly resembles a sinusoidal wave. This condition tends to develop faster for larger odd fractions of the natural frequencies. The resonant behaviour has a higher effect on bristle top stresses than on bristle tip deflection, because the effects of higher modes on stresses are more appreciable. In addition, for a frequency near a natural frequency or far from odd fractions of them, higher stresses and deflections tend to occur for higher values of b. When the frequency is near an odd fraction of a natural frequency, the value of b affects bristle response in a more complex way. Maximum top stresses and tip deflections may increase when b is modified from $\sim$0.5 to either 0 or 1, or they may tend to increase with increasing b in the whole interval (0, 1), depending on the strength or weakness of the resonant behaviour. It was also shown that bristle wear has a profound effect on brush behaviour. For the range of frequencies studied, the first two modes greatly dominate the dynamics of the bristle for frequencies far from odd fractions of the natural frequencies of the bristle, and higher modes become dominant for the VAP function at frequencies close to odd fractions of the natural frequencies. Finally, the patterns of bristle vibration presented in this work also occur in the case of small transverse vibrations of a 2-D cantilever beam. The VAP wave can generate a condition similar to resonance when the frequency is an odd fraction of the natural frequency of the beam. This enables to excite a certain mode with a small frequency. In addition, the resonant response can be varied by modifying the smoothness parameter, by small changes in frequency about a particular odd fraction of a given natural frequency, and/or by selecting a different odd fraction or natural frequency.

Acknowledgements

This work has been supported by the Universidad Tecnológica de Pereira, the University of Surrey, and the Programme Alβan, European Union Programme of High Level Scholarships for Latin America, identification number *(E03D04976CO)*. The authors are also very grateful for the valuable comments provided by the anonymous reviewers. L. V. Vanegas Useche also has to acknowledge being Associate Professor at the Universidad Tecnológica de Pereira.

References

[1] G. Peel, G.M. Michielen, G. Parker, Some aspects of road sweeping vehicle automation, *2001 IEEE/ASME International Conference on Advanced Intelligent Mechatronics Proceedings*, Vols. I and II, 2001, pp. 337–342.

[2] C. Deery, M. Heanue, S. Deacon, P.G. Robinson, A.D. Walmsley, H. Worthington, W. Shaw, A.-M. Glenny, The effectiveness of manual versus powered toothbrushes for dental health: a systematic review, *Journal of Dentistry* 32 (2004) 197–211.

[3] A. Philipossian, L. Mustapha, Effect of tool kinematics, brush pressure and cleaning fluid pH on coefficient of friction and tribology of post-CMP PVA brush scrubbing processes, *Materials Research Society Symposium Proceedings* 767 (2003) 209–215.

[4] G. Peel, A General Theory for Channel Brush Design for Street Sweeping, PhD Thesis, University of Surrey, 2002.

[5] G.M. Peel, G.A. Parker, Initial investigations into the dynamics of cutting brushes for sweeping, *Journal of Dynamic Systems, Measurement, and Control, Transactions of the ASME* 124 (4) (2002) 675–681.

[6] L.V. Vanegas Useche, M.M. Abdel Wahab, G.A. Parker, Theoretical model for the free-flight behaviour of the bristles of an oscillatory gutter brush for road sweeping, *Proceedings of the XIth International Conference on Vibration Engineering*, Timisoara, Romania, September 2005, pp. 83–90.

[7] C. Wang, Brush Modelling and Control Techniques for Automatic Debris Removal During Road Sweeping, PhD Thesis, University of Surrey, 2005.

[8] L.V. Vanegas Useche, M.M. Abdel Wahab, G.A. Parker, Theoretical model for the dynamics of an unconstrained cutting brush of a street sweeper, *Proceedings of the Eighth Biennial ASME Conference on Engineering Systems Design and Analysis ESDA 2006*, Turin, July 2006, pp. ESDA2006-95563-1–ESDA2006-95563-10.

[9] L.V. Vanegas Useche, M.M. Abdel Wahab, G.A. Parker, Brush dynamics: models and characteristics, *Proceedings of the Eighth Biennial ASME Conference on Engineering Systems Design and Analysis ESDA 2006*, Turin, July 2006, pp. ESDA2006-95565-1–ESDA2006-95565-10.

[10] R.J. Stango, C.-Y. Shia, Analysis of filament deformation for a freely rotating cup brush, *Journal of Manufacturing Science and Engineering, Transactions of the ASME* 119 (3) (1997) 298–306.

[11] K.D. Murphy, C.L. Lee, The 1:1 internally resonant response of a cantilever beam attached to a rotating body, *Journal of Sound and Vibration* 211 (2) (1998) 179–194.

[12] B.O. Al-Bedoor, M.N. Hamdan, Geometrically non-linear dynamic model of a rotating flexible arm, *Journal of Sound and Vibration* 240 (1) (2001) 59–72.

[13] B.O. Al-Bedoor, A. El-Sinawi, M.N. Hamdan, Non-linear dynamic model of an inextensible rotating flexible arm supported on a flexible base, *Journal of Sound and Vibration* 251 (5) (2002) 767–781.

[14] T.R. Kane, R.R. Ryan, A.K. Banerjee, Dynamics of a cantilever beam attached to a moving base, *Journal of Guidance, Control, and Dynamics* 10 (2) (1987) 139–151.

[15] H.H. Yoo, R.R. Ryan, R.A. Scott, Dynamics of flexible beams undergoing overall motions, *Journal of Sound and Vibration* 181 (2) (1995) 261–278.

[16] J. Chung, H.H. Yoo, Dynamic analysis of a rotating cantilever beam by using the finite element method, *Journal of Sound and Vibration* 249 (1) (2002) 147–164.

[17] W. Weaver Jr., S.P. Timoshenko, D.H. Young, *Vibrations Problems in Engineering*, fifth ed., Wiley, USA, 1990.